Journal of Insights in Basic and Applied Sciences
مجلة رؤى في العلوم الأساسية والتطبيقية
Volume 2, Issue 4, 2026, Pages: 01-17
Journal homepage: https://jibas.com.ly/index.php/jibas/en

Structure-Based Discovery of Novel PARP1 Inhibitor Candidates Using Pharmacophore Modeling, Virtual Screening, Molecular Docking, and ADMET Profiling

Abdalhamid Alarafi [1*], Haneen A.Wali[2], Raghad AbdulFatah[3] , Naowara Alarafi[4]
[1,3] Department of Chemistry, Faculty of Arts and Sciences, University of Benghazi, Al-Abyar, Libya
[2]Libyan Center for Studies and Research of Environmental Science and Technology, Sabartha, Libya
[4]Department of Chemistry, Faculty of Sciences, University of Benghazi, Benghazi, Libya

اكتشاف مرشحين جدد لمثبطات *PARP1* باستخدام نمذجة Pharmacophore ، والفحص الافتراضي، والالتحام الجزيئي، وتحديد خصائص ADMET

عبد الحميد العرفي[*1]، حنين والي[2] ، رغد عبد الفتاح[3] ، نوارة العرفي[4]
[1،3] قسم الكيمياء، كلية العلوم والاداب، جامعة بنغازي، الأبيار، ليبيا
[2] المركز الليبي لدراسات وبحوث علوم وتكنولوجيا البيئة، صبراتة، ليبيا
[4]قسم الكيمياء، كلية العلوم، جامعة بنغازي، بنغازي، ليبيا

[*]Corresponding author: abdalhamid.abdallah@uob.edu.ly

Received: July 14, 2026	Accepted: October 25, 2026	Published: November 20, 2026

Copyright: © 2026 by the authors. This article is an open-access article distributed under the terms and conditions of the Creative Commons Attribution (CC BY) license (https://creativecommons.org/licenses/by/4.0/).

Abstract:
Poly(ADP-ribose) polymerase 1 (PARP1) is a recognized target for therapy in oncology, especially in cancers with defective homologous recombination repair. Although PARP inhibitors like olaparib have shown clinical effectiveness, the emergence of acquired resistance and associated side effects persistently drive the quest for novel chemical agents. This research utilized a comprehensive structure-based computational method to discover possible PARP1 inhibitors, with olaparib serving as the reference ligand. A pharmacophore model with five features, including three aromatic elements, one hydrogen-bond donor, and one hydrogen-bond acceptor, was created from the crystal structure of the PARP1–olaparib complex (PDB ID: 7KK4) and applied for virtual screening. Chosen compounds were subsequently assessed through molecular docking via MOE 2024, followed by the prediction of their physicochemical, pharmacokinetic, drug-likeness, medicinal chemistry, and toxicity profiles using SwissADME and ProTox 3.0. Re-docking olaparib to validate the docking protocol resulted in an RMSD of 0.992 Å, confirming the dependability of the chosen docking method. Four compounds demonstrated advantageous binding scores between −8.978 and −9.715 kcal/mol, all surpassing that of olaparib (−8.645 kcal/mol). Compound III exhibited the best docking score (−9.715 kcal/mol) and formed several interactions with crucial PARP1 residues, such as Gly863, Tyr896, Ser904, and Tyr907. Each of the four compounds met Lipinski's rule of five and exhibited a predicted bioavailability score of 0.55; however, variations were noted in solubility, CYP inhibition, medicinal chemistry alerts, and anticipated toxicity. The results indicate that Compound III is the most potent binding candidate among the examined series, while also pointing out weaknesses that need structural improvements. These results offer a computational foundation for additional molecular dynamics, binding free-energy assessments, and experimental verification of the discovered PARP1 inhibitor candidates..

Keywords: PARP1, Olaparib, 7KK4, Structure-based pharmacophore, Virtual screening, Molecular docking, ADMET, Drug discovery, SwissADME.

الملخص

يُعد بوليميراز PARP1 (ADP-ribose) هدفًا علاجيًا راسخًا في علاج السرطان، لا سيما في الأورام التي تعاني من خلل في إصلاح إعادة التركيب المتماثل. على الرغم من النجاح السريري لمثبطات PARP1 مثل olaparib ، إلا أن المقاومة المكتسبة والسمية المرتبطة بالعلاج لا تزال تحفز البحث عن مرشحين كيميائيين جدد. في هذه الدراسة، تم استخدام نهج حسابي متكامل قائم على البنية لتحديد مثبطات PARP1 المحتملة باستخدام olaparib كربيطة مرجعية تم توليد نموذج دوائي خماسي الخصائص، يتألف من ثلاث خصائص عطرية، ومانح رابطة هيدروجينية، ومستقبل رابطة هيدروجينية، من البنية البلورية لمركب PARP1-olaparib (معرف بنك بيانات البروتين: KK47)، واستُخدم في الفحص الافتراضي. ثم جرى تقييم مركبات مختارة باستخدام تقنية الإرساء الجزيئي بواسطة برنامج MOE 2024، تلاها التنبؤ بخصائصها الفيزيائية والكيميائية، وحركيتها الدوائية، ومدى ملاءمتها للأدوية، وخصائصها الكيميائية الطبية، وسميتها باستخدام برنامجي SwissADME وProTox 3.0. أظهرت عملية التحقق من صحة بروتوكول الإرساء، من خلال إعادة إرساء olaparib، قيمة RMSD قدرها 0.992 Å، مما يدعم موثوقية إجراء الإرساء المعتمد. أظهرت أربع مركبات درجات ارتباط جيدة تتراوح بين 8.978 و-9.715 كيلو كالوري/مول، متجاوزة جميعها درجة ارتباط olaparib (-8.645 كيلو كالوري/مول). من بينها، أظهر المركب الثالث أفضل نتيجة ارتباط (-9.715 كيلو كالوري/مول) وأقام تفاعلات متعددة مع بقايا PARP1 الرئيسية، بما في ذلك Gly863 وTyr896 وSer904 وTyr907. استوفت جميع المركبات الأربعة قاعدة ليبينسكي الخماسية وأظهرت درجة توافر حيوي متوقعة قدرها 0.55، على الرغم من ملاحظة اختلافات في الذوبانية، وتثبيط CYP، وتنبيهات الكيمياء الطبية، والسمية المتوقعة. بشكل عام، تحدد النتائج المركب الثالث كأقوى مرشح ارتباط ضمن السلسلة المدروسة، مع تسليط الضوء أيضًا على نقاط الضعف التي تتطلب تحسينًا هيكليًا. توفر هذه النتائج أساسًا حسابيًا لمزيد من الديناميكيات الجزيئية، وحسابات طاقة الارتباط الحرة، والتقييم التجريبي لمرشحي مثبط PARP1 المحددين.

الكلمات المفتاحية: PARP1، Olaparib، 7KK4، اكتشاف الأدوية، الالتحام الجزيئي

Introduction

ADP-ribosyl transferases (ARTs) are a structurally conserved group of enzymes that use nicotinamide adenine dinucleotide (NAD^+) as a cofactor to add ADP-ribose units to specific substrate proteins [1, 2]. This modification after translation modulates essential cellular functions, such as enzymatic function, sub-cellular positioning, and multiprotein complex formation [3]. Poly (ADP-ribose) polymerase 1 (PARP1), the most plentiful and well-studied member of this family, serves as a key molecular detector of genomic instability [4]. Upon identifying single-strand DNA breaks (SSBs), PARP1 quickly produces poly (ADP-ribose) (PAR) chains on histones and nuclear targets, successfully attracting the base excision repair (BER) machinery to the sites of damage [5, 6]. Thus, focusing on PARP1 has become a crucial synthetic lethal approach in cancer treatment, especially for tumors with homologous recombination deficiencies, like those with BRCA1 and BRCA2 mutations [7, 8].The pharmacological inhibition of PARP1 hinders the repair of SSBs, leading to their progression into fatal double-strand breaks (DSBs) during the process of DNA replication [9]. Normal cells fix these DSBs through homologous recombination, but cancer cells lacking BRCA1/2 cannot handle them, leading to significant genomic collapse, cell cycle halting, and programmed cell death [10]. Mechanistically, PARP inhibitors function via two separate actions: blocking the catalytic site and spatially "trapping" PARP1 proteins on complexes of damaged DNA [11]. Olaparib is the first FDA-approved PARP inhibitor in its class, showing significant clinical efficacy in the treatment of breast, ovarian, pancreatic, and prostate cancers with BRCA mutations [12].

This research utilized a comprehensive computational workflow that employed Olaparib as a primary structural reference for the creation and analysis of new PARP1 inhibitors. We initially created a structure-based pharmacophore model utilizing the high-resolution crystal complex of the PARP1 catalytic domain complexed with Olaparib (PDB ID: 7KK4), specifying the critical spatial configuration and chemical characteristics required for binding at the active site. Second, comprehensive molecular docking simulations were conducted to examine binding orientations, scoring metrics, and essential non-covalent interaction networks—particularly hydrogen bonds and hydrophobic interactions—inside the catalytic pocket. Ultimately, extensive in silico ADMET profiling (Absorption, Distribution, Metabolism, Excretion, and Toxicity) was performed to assess the pharmacokinetic feasibility, safety margins, and general drug-likeness of the selected candidates. This research creates a logical structure to steer the creation of effective and specific PARP1 inhibitors.

Material and methods

Structure-based pharmacophore modelling

The pharmacophore model based on structure was implemented using the Pharmit webserver (13) to discover potential candidate compounds for PARP1. This analysis utilized the crystal structure of the catalytic domain of human PARP1 (PDB ID: 7KK4), which was determined at a high resolution of 1.96 Å and co-crystallized with olaparib, a reference PARP inhibitor. To determine the optimal pharmacophore features, we analyzed the interactions between the target and the reference. The chosen pharmacophore was subsequently utilized to survey a broad array of databases.

Virtual evaluation and Lipinski's assessment

The chosen pharmacophore model was employed to map databases like MolPort, Chembl, ChemSpace, and purchasable Zinc. The Pharmit webserver hosts these databases, and a filtering process was conducted on the obtained compounds utilizing established drug-likeness criteria, such as molecular weight ≤ 500 Da, LogP ≤ 5, rotatable bonds ≤ 10, polar surface area (PSA) ≤ 140 Å², aromatic rings ≤ 4, hydrogen bond acceptors (HBA) ≤ 10, and hydrogen bond donors (HBD) ≤ 5.

Binding affinity studies

The compounds reduced in the prior step that met the specified pharmacophore and drug-likeness criteria were chosen to evaluate their binding affinity alongside the co-crystallized reference ligand, olaparib. Molecular docking analyses provide insights into the binding mechanism and strength of attachment to the target protein. In this case, MOE 2024 was utilized to assess the binding interactions of the chosen compounds at the active site of PARP1. The crystal structure of human PARP1 (PDB ID: 7KK4), co-crystallized with olaparib, was utilized in this study. The framework was created by eliminating water molecules and irrelevant heteroatoms. The binding pocket was designated around the co-crystallized ligand olaparib, and all docking computations were then performed within this binding area. As a result, the significant residues identified were Asp766, Tyr710, Leu769, Asp770, Trp861, His862, Gly863, Arg878, Ala880, Pro881, Gly894, Ile895, Tyr896, Phe897, Ala898, Lys903, Ser904, Tyr907, and Glu988. These residues were deemed crucial for assessing ligand-binding interactions. The binding poses obtained were evaluated using docking scores and molecular interactions involving the active-site residues, and the results were then compared to those of the reference ligand, olaparib, to find the most promising candidate compounds.

Computing pharmacokinetics, drug-likeness, medicinal chemistry, and toxicity properties

The small molecules exhibiting favorable binding affinity scores underwent calculations of various properties, including physicochemical properties, lipophilicity, water solubility, pharmacokinetic properties, drug-likeness properties, and medicinal chemistry attributes using the web tool SwissADME [14]. Moreover, the toxicity evaluation was conducted utilizing the ProTox 3.0 web server[15, 16].

Physicochemical properties

The physicochemical characteristics provide insight into the overall description of a molecule that is crucial for filtering compounds [14] and serve as a fundamental measure of quality [17]. The OpenBabel API version 2.3.0 [18] is used to calculate these parameters, and the topological polar surface area (TPSA) was determined based on an earlier study [19]. The parameters calculated include molecular refractivity (MR), polar surface area (PSA), and molecular weight (MW). The section on physicochemical properties also addresses the atom count, which comprises the total of aromatic heavy atoms, heavy atoms, hydrogen bond donors, hydrogen bond acceptors, rotatable bonds, and Fraction Csp3. In a specific molecule, the Fraction Csp3 indicates the proportion of sp3-hybridized carbon atoms to the overall count of carbons in that molecule. A molecule possessing a greater Fraction Csp3 value leads to their metabolism and consequently their removal from the body [20]. Moreover, the compound featuring a high Fraction Csp3 exhibits lower toxicity and improved oral bioavailability, thereby enhancing its pharmacological properties. In a similar manner, for optimal oral bioavailability, the Fraction Csp3 is said to range from 0.25 to 1 [21]. Additionally, the molecular weight must be less than 500 Da, the count of rotatable bonds should not exceed 10, the number of hydrogen bond donors must be under 5, and hydrogen bond acceptors should remain below 10. The molar refractivity normally falls between 40 and 130 m³/mol. The molar refractivity indicates the overall polarizability of a substance determined using density, refractive index, and molecular

weight. The TPSA assesses the polarity of the compound and provides insight into whether the compound can cross the biological membranes to enter the cells.

Lipophilicity

Lipophilicity is another key parameter calculated, which influences the pharmacokinetic characteristics of a specific compound. This is referred to as the partition coefficient between n-octanol and water (log P o/w) [14]. This characteristic provides insight into a compound's capacity to dissolve in non-polar solvents or oils. Proposed drug candidates with increased lipophilicity hold significant importance since the targets are lipid-based [23]. Lipophilicity is referred to as the 'logarithm of the partition coefficient between oil and water phases, Log Po/w. The web server computes various lipophilicity techniques including iLOGP, XLOGP3, WLOGP, MLOGP, SILICOS-IT, but the consensus logP o/w is regarded as the standard for assessing a compound's lipophilicity. To be considered potential drugs, compounds typically have an optimal logP o/w value ranging from 1 to 3. Compounds within this range typically exhibit an optimal balance of solubility and permeability, rendering them appropriate for oral use with high bioavailability [21]. The SwissADME, however, establishes the XLOGP3 range as being between -0.7 and +5.0 [24,25].

Solubility

In addition, water solubility is calculated using Log S (ESOL) [26], Log S (Ali) [27], and Log S (SILICOS-IT). Solubility is a measure of the pharmacokinetic properties of compounds. The compounds that are readily soluble can easily dissolve in gastrointestinal fluids, thus enhancing their capacity for oral absorption. These substances stay in a watery environment that results in reduced volume distribution, restricting their ability to penetrate the tissues. To assess the solubility of a specific compound, ESOL is utilized. Greater Log S values, especially those nearer to zero, suggest improved predicted aqueous solubility. These compounds exhibit significant solubility and can be effectively absorbed; a lack of this results in poor solubility [21]. Compounds that show low solubility are eliminated before entering the bloodstream. This characteristic determined the oral uptake of a medication [23].

Pharmacokinetic characteristics

Absorption in the gastrointestinal (GI) tract

It is a process that clarifies the compound's transit through various membranes starting from the site of administration [21]. The absorption of the drug is influenced by the architecture of the gastrointestinal system, the dosage formulation, and its physiochemical characteristics [28]. Compounds exhibiting high GI absorption are favored as potential drug candidates.

Penetration of the blood-brain barrier (BBB)

This is a method to determine if the compounds cross the BBB. Substances that dissolve in lipids can easily traverse this barrier.

P-glycoprotein (P-gp)

The P-glycoprotein protects the body against harmful and external agents. A compound that is not a substrate of P-gp can effectively traverse the P-gp barrier [29]. These compounds show excellent bioavailability [21]. Moreover, increased levels of P-gp in cancer cells lead to multidrug resistance [30].

Elimination

The removal of the drug takes place through biotransformation during metabolism, with cytochromes P450 (CYP) playing a crucial role in this process. Inhibiting isoenzymes leads to drug-drug interactions that produce negative effects due to decreased drug clearance [14]. The enzymes responsible for drug metabolism play a critical role in determining a drug's pharmacokinetic characteristics [31]. The P-gp and CYP collaborate on small molecules to create an enhanced barrier for tissues and organisms. In this investigation, the effects of the isolated compound on five CYPs, which include CYP1A2 inhibitor, CYP2C19 inhibitor, CYP2C9 inhibitor, CYP2D6 inhibitor, and CYP3A4 inhibitor, are estimated [14].

Log kp (skin permeation)

Skin permeability is an additional factor predicted by SwissADME aimed at forecasting the skin permeability coefficient (K) of a specific compound. This forecast aligned with Kp, which had a linear correlation with both lipophilicity and molecular size. The anticipated skin permeability coefficient is denoted as log Kp. Lower negative log Kp values suggest higher predicted skin permeability, while more negative values imply reduced predicted permeability. Of the assessed ligands, ligand II exhibited the greatest predicted skin permeability (log Kp = −6.17), while ligand I had the least predicted skin permeability (log Kp = −8.17) [14,32].

Drug-likeness

Lipinski's rule

Lipinski's "rule of five" is a crucial factor in drug development and indicates whether a compound may be effective when taken orally. Thus, a compound must have at most 5 hydrogen bond donors, at most 10 hydrogen bond acceptors, a molecular weight not exceeding 500 Da, and a LogP of no more than 5. Exceeding this upper limit might indicate inadequate absorption of a proposed compound [33–34].

Ghose's rule

Ghose et al. identified a set of physicochemical characteristics that a compound must exhibit to possess drug-like properties while analyzing the Comprehensive Medicinal Chemistry (CMC) database. Thus, the calculated log P is expected to lie between 0.4 and 5.6, the molecular weight (MW) should be within 160 to 480, the range of molar refractivity should be from 40 to 130, and the total atom count should fall between 20 and 70. It is also indicated that the commonly available substructure is benzene, with prominent functional groups comprising alcoholic OH, tertiary aliphatic amines, and carboxamides [35].

Veber's rule

Veber's rule suggests that a compound with rotatable bonds ≤ 10 and polar surface area ≤ 140 Å² (with 12 or fewer hydrogen bond donors and acceptors) indicates the potential for enhanced bioavailability [36].

Egan's rule

Egan's rule states that a compound can have a maximum AlogP98 value of 5.88 and a TPSA value of 131.6 Å² [37,38].

Muegge's rule

Muegge's rule states that a compound must possess a molecular weight between 200 and 600, a TPSA of 150 or less, more than 4 carbons, 15 or fewer rotatable bonds, no more than 5 hydrogen bond donors, at most 10 hydrogen bond acceptors, a LogP between 2 and 5, a maximum of 7 rings, and more than 1 heteroatom (NH) [38,39].

Bioavailability score

The total quantity of the compound or medication that arrives at the intended site fully is known as bioavailability. This means that the proportion of the drug that arrives in the systemic circulation unchanged and in its active form. Bioavailability is typically measured on a scale from 0 to 1 and is often expressed as a percentage [21,40]. SwissADME computes the bioavailability score based on the work of Martin et al. [41]. A bioavailability score of 0.55 is considered acceptable as long as the rule of five is not violated [41-43].

Medicinal chemistry

PAINS

Pan Assay Interference Ligands (PAINS) are compounds containing substructures that show encouraging outcomes irrespective of the protein target, resulting in false positives [14,44]. Additionally, different assay techniques indicate that these compounds are active and are used as starting points for subsequent studies [24].

Brenk

This parameter is used to analyze the structural characteristics to determine whether a specific compound contains any fragment that might be metabolically unstable, toxic, chemically reactive, resulting in diminished pharmacokinetics [14,45,46]. The PAINS and Brenk outcomes are presented as alerts in the SwissADME evaluation.

Leadlikeness

Lead-like compounds or drugs exhibit a molecular weight under 300. This molecular weight aligns with the molecular weight of the rule of three (Ro3) and is regarded as the upper threshold for lead-like compounds [47]. These compounds offer a potential to evolve into a therapeutic agent [21]. The primary compounds must engage in non-covalent interactions without any identified toxicophoric and be appropriate for structure–activity relationship studies [48]. A compound is deemed a lead if it meets these requirements: hydrogen bond acceptors ≤ 6, hydrogen bond donors ≤ 3, LogP (XLogP3): 1–3, molecular weight between 250–350 Da, rotatable bonds ≤ 7, TPSA ≤ 90 Å 2 [21].

Synthetic availability

The synthetic accessibility score provides insight into the synthesis potential of a specific compound. It assesses whether the specified compound can be synthesized with ease, with results shown as 1 for easy and 10 for very challenging, according to the fragment's contribution and the complexity of the compound [49].

Organ toxicity prediction

The ProTox 3.0 web server was used to predict the organ toxicity of the compounds. In this instance, hepatotoxicity, neurotoxicity, nephrotoxicity, respiratory toxicity, and cardiotoxicity are calculated. The harmful amounts are also expressed in terms of (lethal dose) LD 50 mg/kg of body mass. It refers to a dose that causes the death of 50% of subjects in laboratory experiments. The active and inactive compounds are forecasted based on likelihood, and the forecasts are represented using a color code. The dark green color denotes an inactive probability ≥ 0.7, whereas a light green color represents an inactive probability < 0.7. The active probability of ≥ 0.7 is shown in red, whereas the active probability of < 0.7 is shown in pink [16]. According to the dosage, the lethal categories are classified into six groups: class I: fatal (LD 50), class II: fatal (5 < LD 50 ≤ 50), class III: toxic (50 < LD 50 ≤ 300), class IV: harmful if swallowed (300 < LD 50 ≤ 2000), class V: may be harmful if swallowed (2000 < LD 50 ≤ 5000), and class VI: non-toxic (LD 50 > 5000) [15,16].

Results and discussion

Structure-based pharmacophore modelling

A five-feature pharmacophore model was created using Pharmit. The structure includes three aromatic characteristics, a single hydrogen bond donor, and a single hydrogen bond acceptor (Fig. 1A). The feature of the hydrogen bond donor was complementary to the Gly 863 residue, while the feature of the hydrogen bond acceptor was complementary to the Tyr 896 residue. The three aromatic characteristics complemented residues such as Lys 903 and Tyr 896 (Fig. 1B). This model was employed to conduct pharmacophore-based virtual screening of extensive compound libraries to discover new possible PARP1 inhibitors.

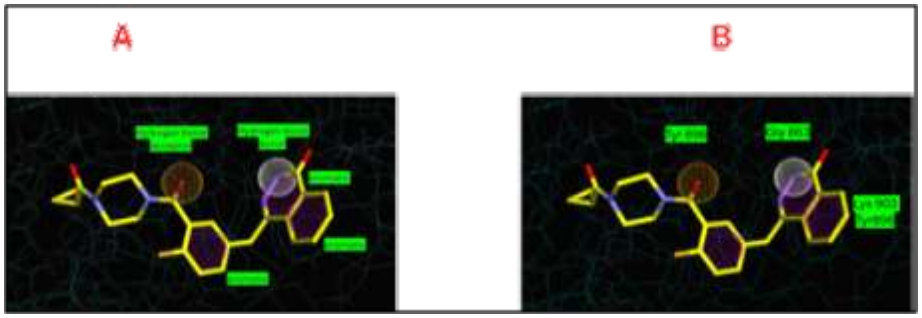

Figure 1. Pharmacophore model with corresponding amino acids residues. 1A) Inbound ligand with pharmacophore features consisting of 3 aromatic features, 1 hydrogen bond donor, and 1 hydrogen bond acceptor. 1B) Amino acid residues corresponding to the pharmacophore features.

Virtual screening and filtering

The pharmacophore model was utilized to screen databases such as MolPort, Chembal36, ChemSpace, and Zinc purchasable, yielding a total of 232,160 compounds. After the Ro5 filters were applied to these compounds, the overall count decreased to 94,437 (Fig. 2).

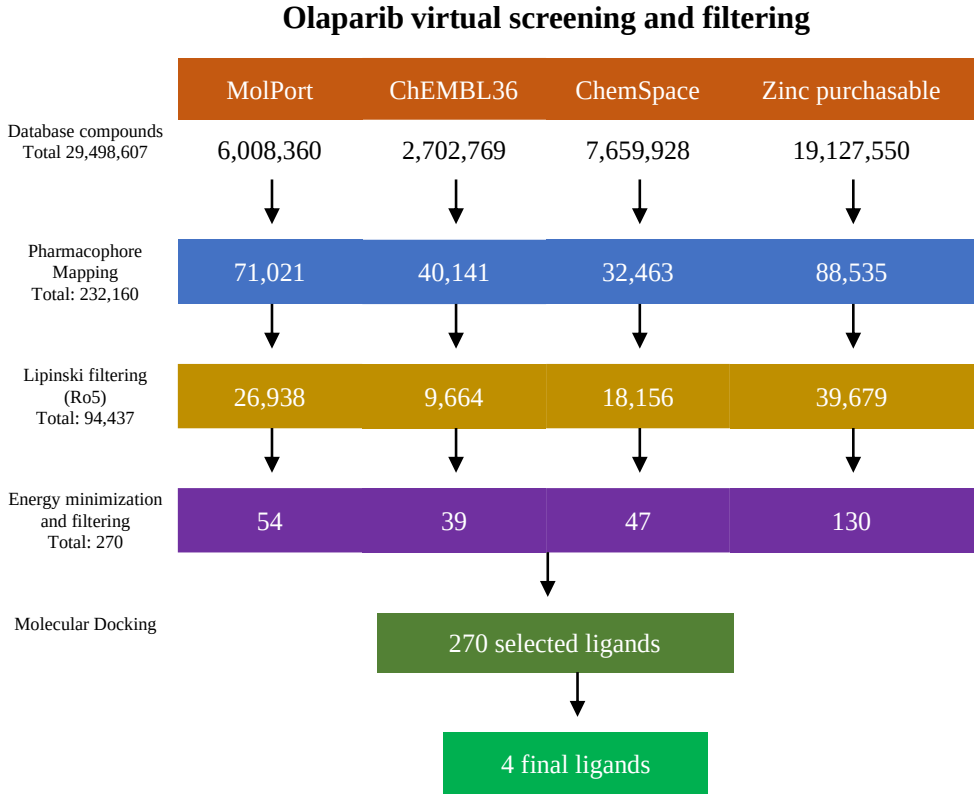

Figure 2. Pharmacophore-based virtual screening and sequential filtering workflow for the identification of potential PARP1 inhibitors.

The filters utilized in this context adhere to Lipinski's rule, a criterion for potential drug candidates [33]. The resulting compounds were optimized to showcase the minimized RMSD (1) and binding affinity score (-9), leading to a total of 270 hits. The compounds exhibiting the highest binding affinity scores were analyzed in more detail (Fig. 2).

Studies on Binding Affinity

Molecular docking analyses were conducted with MOE 2024 to assess the binding affinity of the chosen compounds to the target protein. The docking protocol was confirmed via a re-docking procedure of the co-crystallized ligand into the binding site. The calculated RMSD value of 0.9915 Å, falling below the accepted limit of 2.0 Å, validated the trustworthiness and precision of the docking protocol. Additionally, PyMOL was utilized to illustrate the binding orientations and examine protein-ligand interactions in the active site; four compounds, CHEMBL5632703 (Ligand I), CHEMBL5631466 (Ligand II), CHEMBL6060011 (Ligand III), and ZINC000021332049 21332049 PubChem-135941856 (Ligand IV) exhibited increased binding affinities, and these compounds were further evaluated alongside the reference compound. Ligand I, ligand II, ligand III, and ligand IV exhibited a lower dock score compared to the reference (Table 1). Additionally, ligand I, ligand II, ligand III, and ligand IV have filled the binding pocket (Fig3) in a comparable manner to the crystallized ligand, engaging in

various critical residue interactions. This result suggests that the hits could serve as potential inhibitors for targeting PARP1.

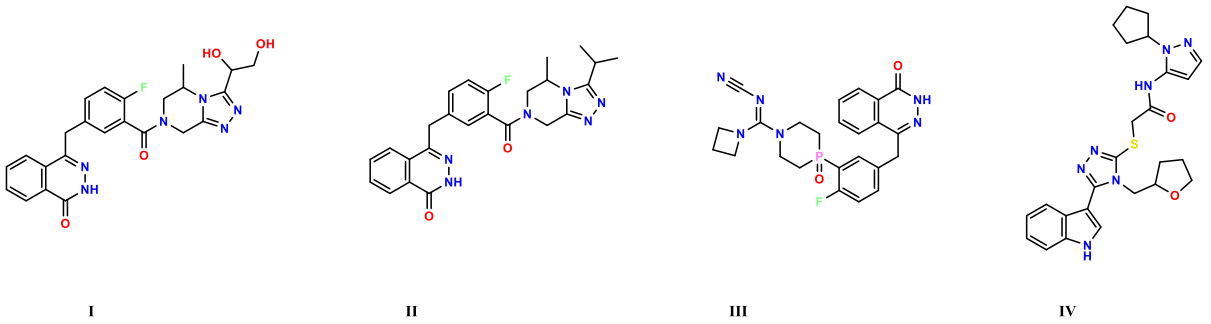

Figure 3. Chemical structures of the four selected ligands (I–IV) identified through pharmacophore-based virtual screening as potential PARP1 inhibitors.

Molecular interactions of ligands

Docking Protocol Validation

The molecular docking protocol was validated by re-docking the co-crystallized ligand Olaparib Drug into the binding sites of the selected proteins. As shown in Table 1, the obtained S-scores/RMSD values were −8.645 kcal/mol/ 0.992Å for7KK4, All RMSD values were below 2.5 Å, confirming the reliability of the docking protocol and its ability to reproduce the experimentally observed binding modes of the reference ligands, according to the co-crystallized ligand Olaparib Drug The corresponding ligand–residue interactions are presented in Table 3.

Table 1: The results obtained from docking validation with Receptor 7KK4

Receptors	Atom of compound	Atom of receptor	Hydrophobic interaction	Receptor Residue	Interaction Type	Distance (Å)	Energy kcal/mol	S score kcal/mol
7KK4	OAC 43	N	Ala876,Trp861,phe897,lle879,Ala880,pro851,Leu877,Leu760.	TYR 896 (A)	H-acceptor	3.03	-5.1	−8.645
	OAD 44	CE		LYS 903 (A)	H-acceptor	3.37	-0.5	

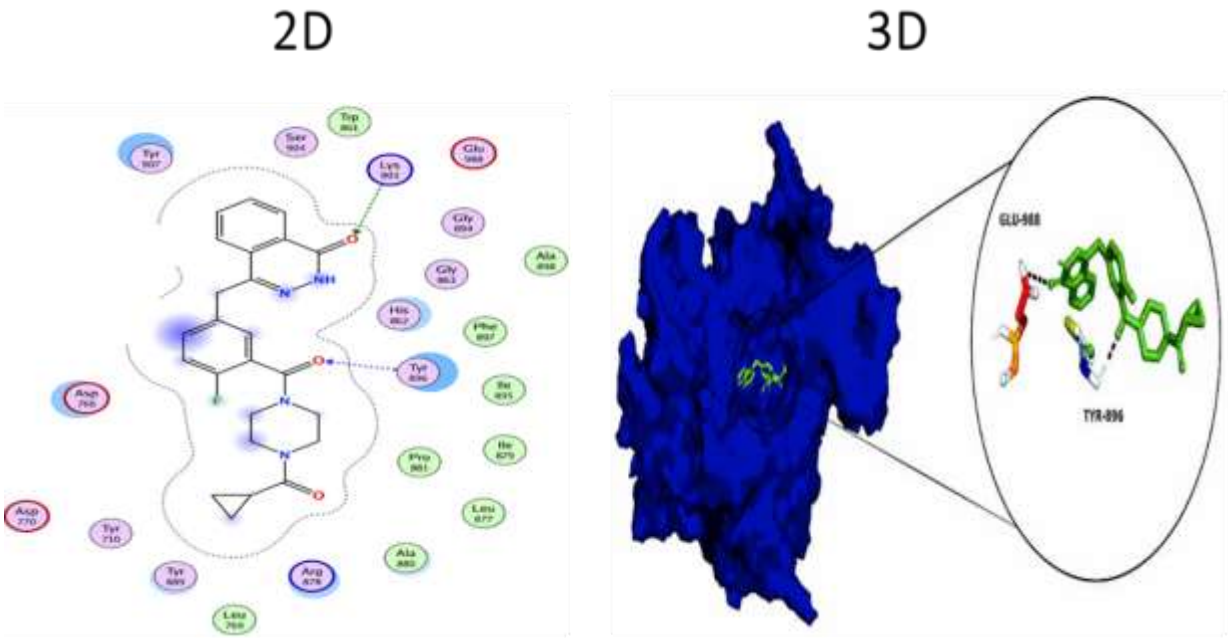

Fig 4: 2D,3D interaction of the docking Reference Ligand with 7KK4

Table 2 : Redocking Validation of co-crystallized ligand of the studied Proteins

Protein	PDB ID	RMSD (Å)	Superimposition plot
Poly [ADP-ribose] polymerase 1 (PARP1) in complex with the PARP inhibitor olaparib	7KK4	0.992	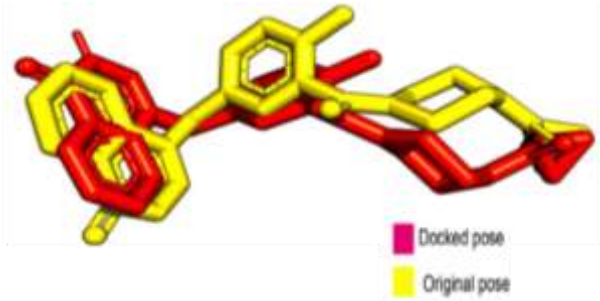

Table 3. Molecular docking results of the pharmacophore-derived compounds with 7KK4.

Ligand	Atom of compound	Atom of receptor	Receptor Residue	Hydrophobic interactions	Interaction Type	Distance (Å)	Energy (kcal/mol)	S score (kcal/mol)	RMSD (Å)
I	O 12	N	TYR 896(A)	Trp861,phe897,leu877,lle897,Ala880,leu796,pro881	H-acceptor	3.05	-4.1	-8.978	1.853
	O 54	CE	LYS 903(A)		H-acceptor	3.42	-0.5		

II	N 53 O 12 O 55 O 55 6-Ring 6-Ring 6-Ring	O N N OG CE 6-Ring 6-Ring	GLY 863(A) TYR 896(A) GLY 863(A) SER 904(A) LYS 903(A) TYR 896(A) TYR 907(A)	Ala898,Trp861,phe897,leu877,lle897,Ala880,leu796,pro881	H-donor H-acceptor H-acceptor H-acceptor H–π π -π π -π	2.88 2.94 3.03 2.87 4.84 3.99 3.95	-6.1 -4.1 -4.2 -2.3 -0.55 -0.0 -0.0	-9.586	1.855
III	N 45 O 12 O 47 O 47 6-Ring 6-Ring 6-Ring	O N N OG CB 6-Ring 6-Ring	GLY 863(A) TYR 896(A) GLY 863(A) SER 904(A) TYR 896(A) TYR 896(A) TYR 907(A)	lle872, lle892, Ala898,Trp861,phe897,leu877,Ala880,leu796,pro881	H-donor H-acceptor H-acceptor H-acceptor H–π π -π π -π	2.94 3.03 3.03 2.95 4.04 3.90 3.82	-6.2 -3.8 -4.2 -2.0 -0.5 -0.0 -0.0	-9.715	1.350
IV	5-Ring	6-Ring	TYR 907(A)	phe897,leu877,Ala880,leu796,pro881	π -π	3.92	-0.0	-9.181	1.450

Molecular docking study of the four examined compounds against 7KK4 revealed S-scores between −9.715 and −8.978 kcal/mol and RMSD values from 1.350 to 1.853 Å. Compound I displayed an S-score of −8.978 kcal/mol with an RMSD of 1.853 Å, while Compounds II, III, and IV had S-scores of −9.586, −9.715, and −9.181 kcal/mol, along with RMSD values of 1.855, 1.350, and 1.450 Å, respectively. Of the four compounds, Compound III demonstrated the best S-score (−9.715 kcal/mol) along with the lowest RMSD (1.350 Å) and was thus chosen for comparison to the co-crystallized Olaparib drug, which had an S-score of −8.645 kcal/mol and an RMSD of 0.992 Å.

Compound III exhibited multiple advantageous interactions, featuring an H-donor interaction with GLY863 at 2.94 Å (−6.2 kcal/mol) and H-acceptor interactions with TYR896, GLY863, and SER904 at distances of 3.03, 3.03, and 2.95 Å, with respective interaction energies of −3.8, −4.2, and −2.0 kcal/mol. Moreover, H–π and π–π interactions were noted with TYR896 and TYR907 at distances of 4.04, 3.90, and 3.82 Å. In comparison, the Olaparib Drug established H-bond interactions with TYR896 and LYS903 at distances of 3.03 and 3.37 Å, with interaction energies of −5.1 and −0.5 kcal/mol, respectively. Both Compound III and Olaparib Drug notably interacted with TYR896 at a distance of 3.03 Å, whereas Compound III showed extra hydrogen-bonding, H–π, π–π, and hydrophobic interactions. While Olaparib displayed a reduced RMSD (0.992 Å), suggesting a conformation nearer to the crystallographic ligand, Compound III exhibited a more advantageous S-score (−9.715, −8.645 kcal/mol) and a wider interaction profile. These results highlight Compound III as the most advantageous compound among the four examined ligands based on the integrated evaluation of S-score, RMSD, and interaction pattern compared to Olaparib Drug.

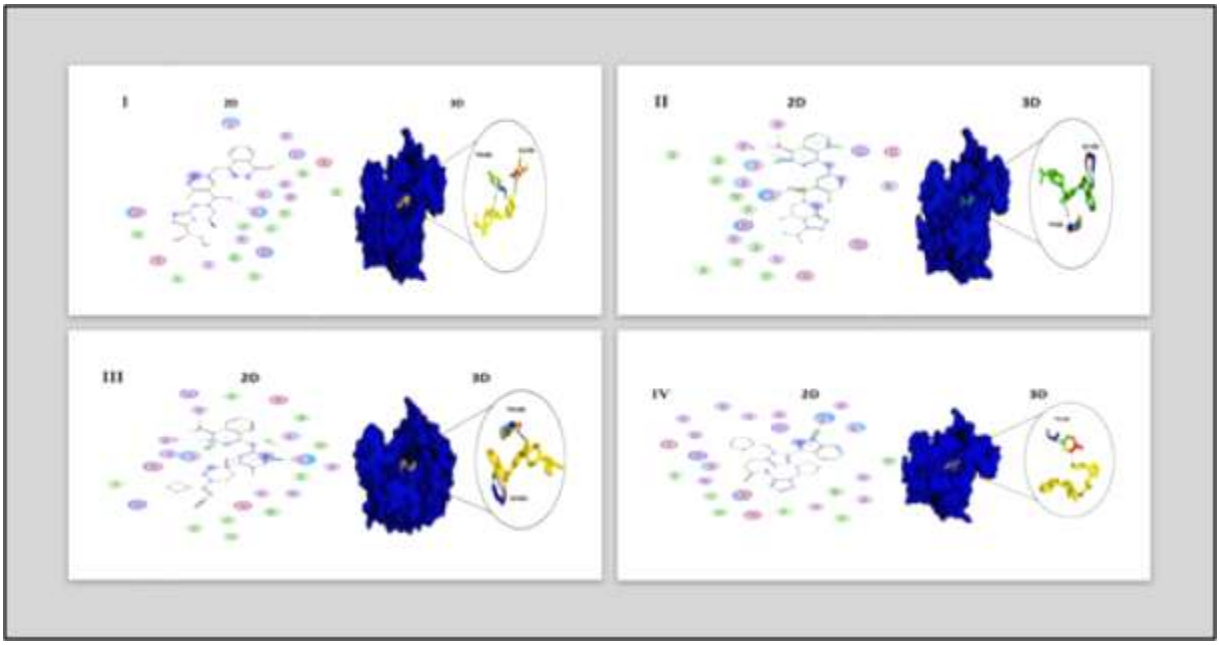

Figure 5. shows the 2D and 3D interaction between ligands I,II III,IV of 7KK4 Receptor

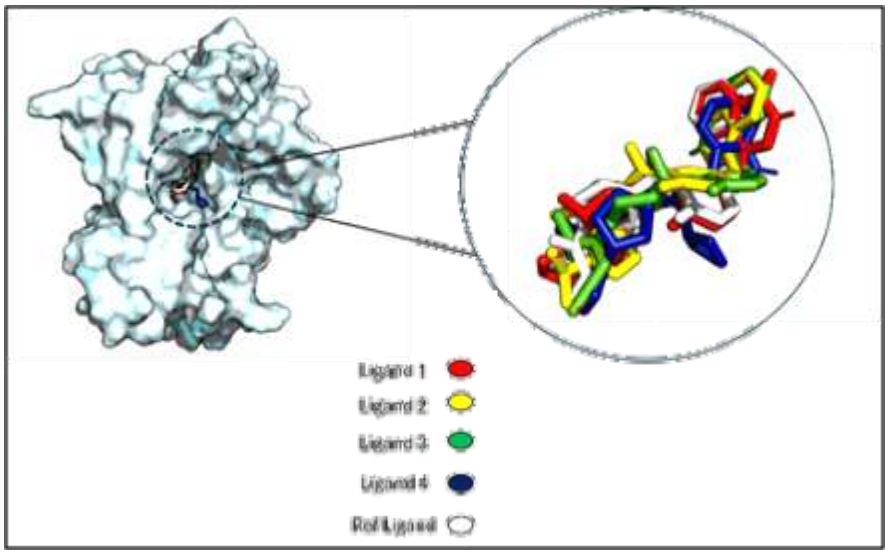

Figure 6. Accommodation of the ligands at the binding pocket of the target protein

Computing pharmacokinetics, drug-likeness, medicinal chemistry, and toxicity properties

The obtained compounds (ligands) were evaluated for their characteristics including physicochemical properties, lipophilicity, water solubility, pharmacokinetic properties, drug-likeness properties, and medicinal chemistry properties using a free online tool SwissADME [14]. Additionally, the toxicity assessment was conducted using the ProTox 3.0 online platform [15,16].

Table 4. Physicochemical, pharmacokinetics and ADMET predictions of ligands

		Ligand I	Ligand II	Ligand III	Ligand IV
Physicochemical Properties	Formula	C24H23FN6O4	C25H25FN6O2	C24H24FN6O2P	C25H29N7O2S
	Molecular weight	478.48 g/mol	460.50 g/mol	478.46 g/mol	491.61 g/mol
	Num. heavy atoms	35	34	34	35
	Num.arom. heavy atoms	21	21	16	19
	Fraction Csp3	0.29	0.32	0.33	0.44
	Num. rotatable bonds	6	5	5	9
	Num. H-bond acceptors	8	6	6	5
	Num. H-bond donors	3	1	1	2
	Molar Refractivity	127.71	130.19	137.22	136.49
	TPSA	137.23 Å²	96.77 Å²	115.26 Å²	127.95 Å²
Lipophilicity	Log $P_{o/w}$ (iLOGP1.5)	1.97	2.47	3.23	2.63
	Log $P_{o/w}$ (XLOGP3)	1.48	4.14	3.13	3.12
	Log $P_{o/w}$ (WLOGP)	1.05	3.47	2.16	4.46
	Log $P_{o/w}$ (MLOGP)	1.46	3.22	2.78	2.74
	Log $P_{o/w}$ (SILICOS-IT)	0.61	2.22	3.09	-0.01
	Consensus Log $P_{o/w}$	1.31	3.10	2.88	2.59
Water Solubility	Log S (ESOL)	-3.79	-5.43	-4.80	-4.66
	Solubility	7.81e-02 mg/ml ; 1.63e-04 mol/l	1.71e-03 mg/ml ; 3.71e-06 mol/l	7.64e-03 mg/ml ; 1.60e-05 mol/l	1.07e-02 mg/ml ; 2.18e-05 mol/l
	Class	Soluble	Moderately soluble	Moderately soluble	Moderately soluble
	Log S (Ali)	-3.97	-5.88	-5.22	-5.48
	Solubility	5.14e-02 mg/ml ; 1.07e-04 mol/l	6.08e-04 mg/ml ; 1.32e-06 mol/l	2.89e-03 mg/ml ; 6.03e-06 mol/l	1.64e-03 mg/ml ; 3.34e-06 mol/l
	Class	Soluble	Moderately soluble	Moderately soluble	Moderately soluble
	Log S (SILICOS-IT)	-5.70	-7.24	-6.78	-4.67
	Solubility	9.46e-04 mg/ml ; 1.98e-06 mol/l	2.64e-05 mg/ml ; 5.73e-08 mol/l	7.98e-05 mg/ml ; 1.67e-07 mol/l	1.05e-02 mg/ml ; 2.13e-05 mol/l
	Class	Moderately soluble	Poorly soluble	Poorly soluble	Moderately soluble

Pharmacokinetics	GI absorption	High	High	High	Low
	BBB permeant	No	No	No	No
	P-gp substrate	Yes	Yes	Yes	Yes
	CYP1A2 inhibitor	No	No	No	No
	CYP2C19 inhibitor	No	Yes	Yes	Yes
	CYP2C9 inhibitor	No	Yes	Yes	Yes
	CYP2D6 inhibitor	No	No	No	Yes
	CYP3A4 inhibitor	No	Yes	Yes	Yes
	Log Kp (skin permeation)	-8.17	-6.17	-7.00	-7.08
Druglikeness	Lipinski	Yes; 0 violation	Yes; 0 violation	Yes; 0 violation	Yes; 0 violation
	Ghose	Yes	No; 1 violation: MR>130	No; 1 violation: MR>130	No; 2 violations: MW>480, MR>130
	Veber	Yes	Yes	Yes	Yes
	Egan	No; 1 violation: TPSA>131.6	Yes	Yes	Yes
	Muegge	Yes	Yes	Yes	Yes
	Bioavailability Score	0.55	0.55	0.55	0.55
Medicinal Chemistry	PAINS	0 alert	0 alert	0 alert	0 alert
	Brenk	0 alert	0 alert	4 alerts: cyanate_aminonitrile_thiocyanate, imine_1, imine_2, phosphor	0 alert
	Leadlikeness	No; 1 violation: MW>350	No; 2 violations: MW>350, XLOGP3>3.5	No; 1 violation: MW>350	No; 2 violations: MW>350, Rotors>7
	Synthetic accessibility	4.47	4.17	4.71	4.38
Organ toxicity prediction	Predicted LD50/ Toxicity Class	Predicted LD50: 500mg/kg Predicted Toxicity Class: 4	Predicted LD50: 500mg/kg Predicted Toxicity Class: 4	Predicted LD50: 500mg/kg Predicted Toxicity Class: 4	Predicted LD50: 1000mg/kg Predicted Toxicity Class: 4
	Hepatotoxicity	Inactive 0.52	Inactive 0.60	Inactive 0.61	Inactive 0.52
	Neurotoxicity	Active 0.78	Active 0.85	Active 0.72	Active 0.69
	Nephrotoxicity	Active 0.52	Inactive 0.66	Inactive 0.57	Active 0.55
	Respiratory toxicity	Active 0.90	Active 0.88	Active 0.81	Active 0.90
	Cardiotoxicity	Inactive 0.80	Inactive 0.88	Inactive 0.81	Inactive 0.84

Journal of Insights in Basic and Applied Sciences
مجلة رؤى في العلوم الأساسية والتطبيقية
Volume 2, Issue 4, 2026, Pages: 01-17
Journal homepage: https://jibas.com.ly/index.php/jibas/en

The findings in Table 4 emphasize the variations in the anticipated developability of the four ligands, which are not noticeable from their docking scores alone. Even though all ligands met Lipinski's rule of five, variations existed in their solubility, gastrointestinal absorption, CYP inhibition profiles, and medicinal chemistry alerts. These results establish a foundation for prioritizing experimental research while determining characteristics that might need structural enhancement.

The molecular weights varied from 460.50 to 491.61 g/mol, with each ligand staying under 500 g/mol. The counts of their hydrogen-bond donors and acceptors were likewise in agreement with Lipinski's rules. However, the comparatively high molecular weights allow for little flexibility in adding substituents during optimization without surpassing this limit. Ligand IV exhibited the highest molecular weight and the most significant conformational flexibility, possessing nine rotatable bonds, whereas the other ligands had five or six. Fraction Csp3 values varied between 0.29 and 0.44, with ligand IV exhibiting the greatest percentage of sp3-hybridized carbon atoms. These variations outline the structural features of the series but do not alone confirm advantageous pharmacokinetic properties.

Polarity and molar refractivity explained various discrepancies among the drug-likeness filters. Ligand I exhibited the greatest topological polar surface area, measuring 137.23 Å², and successfully met the Veber filter criteria while surpassing the Egan polarity threshold. In contrast, ligands II–IV met the Egan filter criteria but did not satisfy the Ghose filter, as their molar refractivity values were above the allowed maximum; ligand IV also surpassed the molecular-weight limit set by Ghose. The Muegge filter was successfully passed by all four ligands. Consequently, consensus on certain filters coexisted with particular breaches in others, endorsing a property-by-property evaluation instead of a unified categorization of the ligands as appropriate oral medications [14].

The lipophilicity findings indicated that ligand I is the least lipophilic compound in the series, exhibiting a consensus log P of 1.31. The respective values for ligands II, III, and IV were 3.10, 2.88, and 2.59, correspondingly. Ligand II recorded the highest XLOGP3 value, measuring 4.14. In this series, the highest anticipated lipophilicity was associated with the lowest expected aqueous solubility in all three solubility models. Ligand I demonstrated the best solubility predictions, classified as soluble by ESOL and Ali, and moderately soluble by SILICOS-IT. Ligands II and III were categorized as moderately soluble by ESOL and Ali but poorly soluble by SILICOS-IT, while ligand IV was uniformly classified as moderately soluble. The difference among models was significant for certain ligands: the estimated log S for ligand II varied from −5.43 to −7.24. As a result, experimental solubility assessments are essential to determine concentrations appropriate for biological testing and to evaluate if restricted dissolution might hinder further progress.

Gastrointestinal absorption was anticipated to be elevated for ligands I–III and minimal for ligand IV. The outcome for ligand IV is noteworthy as it successfully cleared multiple drug-likeness assessments despite its poor absorption rating. All ligands were anticipated to be substrates of P-glycoprotein, indicating a possible role of efflux in their distribution. None was anticipated to cross the blood–brain barrier. These results must be viewed collectively, as a positive passive absorption forecast does not guarantee sufficient systemic exposure when other disposition-related constraints are present. Likewise, the bioavailability score of 0.55, held by all four ligands, is a screening metric and must not be seen as a calculated or estimated definitive oral bioavailability of 55% [14].

The CYP inhibition profiles offered an additional differentiation among the ligands. Ligand I was forecasted to not block any of the five CYP isoforms evaluated. Ligands II–IV were forecasted to obstruct CYP2C19, CYP2C9, and CYP3A4, whereas ligand IV also displayed predicted inhibition of CYP2D6. No enzyme was expected to block CYP1A2. Ligand I consequently exhibited the least alarming predicted CYP inhibition profile among the assessed panel. Nevertheless, these categorizations fail to measure inhibition strength or determine the probability of a significant drug interaction in clinical settings. Assays measuring inhibition based on concentration would be necessary to assess the significance of these predictions.

The results of medicinal chemistry must be taken into account alongside the docking analysis. No PAINS alerts were found for any ligands, while ligand III produced four Brenk alerts: cyanate_aminonitrile_thiocyanate, imine_1, imine_2, and phosphor. These alerts pinpoint substructures that need further scrutiny; they do not, on their own, prove chemical instability, assay interference, or toxicity [14]. Their existence, however, renders

validation of the input framework and evaluation of the highlighted features especially critical for ligand III. All four ligands did not pass the lead-likeness filter due to their molecular weight, with extra violations related to XLOGP3 for ligand II and the count of rotatable bonds for ligand IV. The scores for synthetic accessibility were quite close, varying between 4.17 and 4.71. These intermediate scores offer a preliminary assessment of synthetic difficulty but do not confirm that the ligands can be easily synthesized or via effective synthetic pathways [49].

The toxicity forecasts highlighted worries that were common throughout the series. All four ligands were categorized as acute oral toxicity class IV, showing predicted LD50 values of 500 mg/kg for ligands I–III and 1000 mg/kg for ligand IV. Even though the later estimate indicates reduced expected acute oral toxicity, it fails to demonstrate a superior overall safety profile. All ligands were estimated to show activity for neurotoxicity and respiratory toxicity. Nephrotoxicity was also forecasted for ligands I and IV, but the corresponding confidence scores of 0.52 and 0.55 suggest significant uncertainty in these assessments. Predictions for hepatotoxicity and cardiotoxicity were inactive for all ligands, though the relatively low confidence scores for hepatotoxicity diminish the assurance offered by these negative predictions. These specific outputs for endpoints should inform additional testing instead of being regarded as proof of confirmed toxicity or safety [16]. The anticipated lack of blood–brain barrier penetration does not alleviate the neurotoxicity warnings, as the two predictions pertain to distinct endpoints.

Taking these findings into account, ligand I presents a fairly advantageous mix of anticipated solubility and CYP inhibitory traits, even though its elevated polarity and toxicity warnings continue to be pertinent drawbacks. Ligand III continues to be noteworthy due to its advantageous docking score, yet its Brenk alerts, inconsistent solubility forecasts, and anticipated inhibition of multiple CYP isoforms hinder its prioritization. Ligand II necessitates careful consideration of solubility and CYP inhibition, whereas ligand IV raises further issues regarding anticipated absorption and conformational flexibility. Consequently, no individual ligand achieves the best outcomes for all assessed characteristics. To establish which ligand offers the best foundation for additional optimization, it is necessary to experimentally confirm PARP1 inhibition and cellular target engagement, along with conducting studies on solubility, permeability, metabolic interactions, and toxicity.

Conclusion

This research utilized a combined pharmacophore-driven virtual screening, molecular docking, and in silico ADMET approach to discover possible PARP1 inhibitors, using olaparib as a clinically validated benchmark. The pharmacophore model based on structure effectively identified important interaction characteristics in the PARP1 catalytic pocket, leading to the selection of four candidate compounds for additional study. The docking protocol's reliability was confirmed by the successful re-docking of olaparib, achieving an RMSD of 0.992 Å.

Each of the four chosen compounds exhibited better docking scores compared to olaparib, suggesting their ability to engage effectively with the PARP1 active site. Compound III was identified as the most promising candidate from the docking analysis, exhibiting an S-score of −9.715 kcal/mol and an RMSD of 1.350 Å. The stabilization of its binding pose was achieved through a network of hydrogen bonds, H–π, π–π, and hydrophobic interactions with crucial residues, especially Gly863, Tyr896, Ser904, and Tyr907. The contact with Tyr896, seen similarly with olaparib, reinforces the capacity of Compound III to occupy an important area of the PARP1 binding pocket.

The ADMET analysis offered another viewpoint on the feasibility of developing the identified ligands. All compounds adhered to Lipinski's rule of five and demonstrated acceptable predicted bioavailability scores, whereas ligands 1–3 displayed elevated predicted gastrointestinal absorption. Nonetheless, the computational evaluation also uncovered constraints that ought not to be ignored. All four compounds were forecasted as P-glycoprotein substrates, several indicated potential CYP inhibition, and Compound III produced four Brenk structural alerts. ProTox 3.0 additionally categorized the compounds into toxicity class IV and forecasted potential neurotoxicity and respiratory toxicity, highlighting that favorable docking by itself is inadequate to confirm therapeutic appropriateness.

Collectively, the current results indicate that ligand III stands out as the most promising binding scaffold among the candidates examined rather than being a verified PARP1 inhibitor. Its advantageous binding characteristics offer a valuable foundation for additional enhancement, especially to tackle the anticipated medicinal chemistry and toxicity concerns. To validate binding stability, inhibitory effect, selectivity, and safety, molecular dynamics simulations, free-energy binding calculations, along with following biochemical and cellular assays, are necessary before these compounds can advance to preclinical development.

References:

[1] Hassa, P. O., & Hottiger, M. O. (2008). The diverse biological roles of mammalian PARPs, a small but powerful family of poly-ADP-ribose polymerases. Frontiers in Bioscience, 13, 3046–3082.

[2] Steffen, J. D., Brody, J. R., Armen, R. S., & Pascal, J. M. (2013). Structural implications for selective targeting of PARPs. Frontiers in Oncology, 3, 301.

[3] Hassa, P. O., Haenni, S. S., Elser, M., & Hottiger, M. O. (2006). Nuclear ADP-ribosylation reactions in mammalian cells: Where are we today and where are we going? Microbiology and Molecular Biology Reviews, 70, 789–829.

[4] D'Amours, D., Desnoyers, S., D'Silva, I., & Poirier, G. G. (1999). Poly(ADP-ribosyl)ation reactions in the regulation of nuclear functions. Biochemical Journal, 342(2), 249–268.

[5] Polo, S. E., & Jackson, S. P. (2011). Dynamics of DNA damage response proteins at DNA breaks: A focus on protein modifications. Genes & Development, 25, 409–433.

[6] Hoeijmakers, J. H. (2001). Genome maintenance mechanisms for preventing cancer. Nature, 411, 366–374.

[7] McGlynn, P., & Lloyd, R. G. (2002). Recombinational repair and restart of damaged replication forks. Nature Reviews Molecular Cell Biology, 3, 859–870.

[8] Bryant, H. E., Schultz, N., Thomas, H. D., Parker, K. M., Flower, D., Lopez, E., Kyle, S., Meuth, M., Curtin, N. J., & Helleday, T. (2005). Specific killing of BRCA2-deficient tumours with inhibitors of poly(ADP-ribose) polymerase. Nature, 434, 913–917.

[9] Farmer, H., McCabe, N., Lord, C. J., Tutt, A. N., Johnson, D. A., Richardson, T. B., Santarosa, M., Dillon, K. J., Hickson, I., Knights, C., Martin, N. M., Jackson, S. P., Smith, G. C., & Ashworth, A. (2005). Targeting the DNA repair defect in BRCA mutant cells as a therapeutic strategy. Nature, 434, 917–921.

[10] Jiang, X., Li, W., Li, X., Bai, H., & Zhang, Z. (2019). Current status and future prospects of PARP inhibitor clinical trials in ovarian cancer. Cancer Management and Research, 11, 4371–4390.

[11] Pilié, P. G., Gay, C. M., Byers, L. A., O'Connor, M. J., & Yap, T. A. (2019). PARP inhibitors: Extending benefit beyond BRCA-mutant cancers. Clinical Cancer Research, 25, 3759–3771.

[12] Murai, J., Huang, S. Y., Das, B. B., Renaud, A., Zhang, Y., Doroshow, J. H., Ji, J., Takeda, S., & Pommier, Y. (2012). Trapping of PARP1 and PARP2 by clinical PARP inhibitors. Cancer Research, 72, 5588–5599.

[13] Sunseri J, Koes DR. Pharmit: interactive exploration of chemical space. Nucleic Acids Res. 2016;44:W442–448. doi:10.1093/nar/gkw287.

[14] Daina A, Michielin O, Zoete V. SwissADME: a free web tool to evaluate pharmacokinetics, drug-likeness and medicinal chemistry friendliness of small molecules. Sci Rep. 2017;7:42717. doi:10.1038/srep42717.

[15] Banerjee P, Eckert AO, Schrey AK, Preissner R. ProTox-II: a webserver for the prediction of toxicity of chemicals. Nucleic Acids Res. 2018;46:W257–263. doi:10.1093/nar/gky318.

[16] Banerjee P, Kemmler E, Dunkel M, Preissner R. ProTox 3.0: a webserver for the prediction of toxicity of chemicals. Nucleic Acids Res. 2024;52:W513–520. doi:10.1093/nar/gkae303.

[17] Bunally SB, Luscombe CN, Young RJ. Using physicochemical measurements to influence better compound design. SLAS Discovery. 2019;24(8):791–801. doi:10.1177/2472555219859845.

[18] O'Boyle NM, Banck M, James CA, Morley C, Vandermeersch T, Hutchison GR. Open Babel: an open chemical toolbox. J Cheminform. 2011;3:33. doi:10.1186/1758-2946-3-33.

[19] Ertl P, Rohde B, Selzer P. Fast calculation of molecular polar surface area as a sum of fragment-based contributions and its application to the prediction of drug transport properties. J Med Chem. 2000;43(20):3714–3717. doi:10.1021/jm000942e.

[20] Rai M, et al. Herbal concoction unveiled: a computational analysis of phytochemicals' pharmacokinetic and toxicological profiles using novel approach methodologies (NAMs). Curr Res Toxicol. 2023;5:100118. doi:10.1016/j.crtox.2023.100118.

[21] Zeki NM, Mustafa YF. Digital alchemy: exploring the pharmacokinetic and toxicity profiles of selected coumarin-heterocycle hybrids. Results Chem. 2024;10:101754. doi:10.1016/j.rechem.2024.101754.

[22] Kralj S, Jukić M, Bren U. Molecular filters in medicinal chemistry. Encyclopedia. 2023. doi:10.3390/encyclopedia3020035.

[23] Chandrasekaran B, Abed SN, Al-Attraqchi O, Kuche K, Tekade RK. Computer-aided prediction of pharmacokinetic (ADMET) properties. In: Advances in Pharmaceutical Product Development and Research. Academic Press; 2018:731–755. doi:10.1016/B978-0-12-814421-3.00021-X.

[24] Ranjith D, Ravikumar C. SwissADME predictions of pharmacokinetics and drug-likeness properties of small molecules present in Ipomoea mauritiana Jacq. J Pharmacogn Phytochem. 2019;8(5):2063–2073.

[25] Cheng T, et al. Computation of octanol-water partition coefficients by guiding an additive model with knowledge. J Chem Inf Model. 2007;47(6):2140–2148.

[26] Delaney JS. ESOL: estimating aqueous solubility directly from molecular structure. J Chem Inf Comput Sci. 2004;44(3):1000–1005.

[27] Ali J, Camilleri P, Brown MB, Hutt AJ, Kirton SB. Revisiting the general solubility equation: in silico prediction of aqueous solubility incorporating the effect of topographical polar surface area. J Chem Inf Model. 2012;52(2):420–428.
[28] Anderson GD, Saneto RP. Current oral and non-oral routes of antiepileptic drug delivery. Adv Drug Deliv Rev. 2012;64(10):911–918. doi:10.1016/j.addr.2012.01.017.
[29] Ahmed Juvale II, Abdul Hamid AA, Abd Halim KB, Che Has AT. P-glycoprotein: new insights into structure, physiological function, regulation and alterations in disease. Heliyon. 2022;8(6):e09777. doi:10.1016/j.heliyon.2022.e09777.
[30] Karthika C, et al. Multidrug resistance of cancer cells and the vital role of P-glycoprotein. Life. 2022;12(6):897. doi:10.3390/life12060897.
[31] Brändén G, Sjögren T, Schnecke V, Xue Y. Structure-based ligand design to overcome CYP inhibition in drug discovery projects. Drug Discov Today. 2014;19(7):905–911. doi:10.1016/j.drudis.2014.03.012.
[32] Potts RO, Guy RH. Predicting skin permeability. Pharm Res. 1992;9(5):663–669. doi:10.1023/A:1015810312465.
[33] Lipinski CA, Lombardo F, Dominy BW, Feeney PJ. Experimental and computational approaches to estimate solubility and permeability in drug discovery and development settings. Adv Drug Deliv Rev. 2012. doi:10.1016/j.addr.2012.09.019.
[34] Roskoski R Jr. Properties of FDA-approved small molecule protein kinase inhibitors. Pharmacol Res. 2019;144:19–50. doi:10.1016/j.phrs.2019.03.006.
[35] Ghose AK, Viswanadhan VN, Wendoloski JJ. A knowledge-based approach in designing combinatorial or medicinal chemistry libraries for drug discovery. J Comb Chem. 1999;1(1):55–68. doi:10.1021/cc9800071.
[36] Veber DF, Johnson SR, Cheng HY, Smith BR, Ward KW, Kopple KD. Molecular properties that influence the oral bioavailability of drug candidates. J Med Chem. 2002;45(12):2615–2623. doi:10.1021/jm020017n.
[37] Egan WJ, Merz KM, Baldwin JJ. Prediction of drug absorption using multivariate statistics. J Med Chem. 2000;43(21):3867–3877.
[38] Alvarado Salazar JA, et al. In silico and in vivo evaluation of novel 2-amino-benzothiazole derivative compounds as antidiabetic agents. 2025. doi:10.3390/ijms26030909.
[39] Vélez LA, Delgado Y, Ferrer-Acosta Y, Suárez-Arroyo IJ, Rodríguez P, Pérez D. Theoretical prediction of gastrointestinal absorption of phytochemicals. 2022. doi:10.3390/ijpb13020016.
[40] Price G, Patel DA. Drug bioavailability. 2020.
[41] Martin YC. A bioavailability score. J Med Chem. 2005;48(9):3164–3170. doi:10.1021/jm0492002.
[42] Udugade SB, Doijad RC, Udugade BV. In silico evaluation of pharmacokinetics, drug-likeness and medicinal chemistry friendliness of momordicin1. J Adv Sci Res. 2019;10:222–229.
[43] Ziemska J, Solecka J, Jaronczyk M. In silico screening for novel leucine aminopeptidase inhibitors with 3,4-dihydroisoquinoline scaffold. 2020. doi:10.3390/molecules25071753.
[44] Baell JB, Holloway GA. New substructure filters for removal of Pan Assay Interference Compounds (PAINS) from screening libraries and for their exclusion in bioassays. J Med Chem. 2010;53(7):2719–2740. doi:10.1021/jm901137j.
[45] Brenk R, et al. Lessons learnt from assembling screening libraries for drug discovery for neglected diseases. ChemMedChem. 2008;3(3):435–444. doi:10.1002/cmdc.200700139.
[46] Prabha B, Ezhilarasi M. Synthesis, spectral characterization, in vitro and in silico studies of benzodioxin pyrazoline derivatives. Biointerface Res Appl Chem. 2020;11:9126–9138.
[47] Raymer B, Bhattacharya SK. Lead-like drugs: a perspective. J Med Chem. 2018;61(23):10375–10384. doi:10.1021/acs.jmedchem.8b00407.
[48] Fattori D. Molecular recognition: the fragment approach in lead generation. Drug Discov Today. 2004;9(5):229–238. doi:10.1016/S1359-6446(03)03007-1.
[49] Ertl P, Schuffenhauer A. Estimation of synthetic accessibility score of drug-like molecules based on molecular complexity and fragment contributions. J Cheminform. 2009;1:8. doi:10.1186/1758-2946-1-8.